RADC-TR-90-177
Final Technical Report
August 1990

FIBER OPTIC SYNTHETIC APERTURE INTERFEROMETER

Optra, Inc.

Michael Hercher

APPROVED FOR PUBLIC RELEASE; DISTRIBUTION UNLIMITED.

This effort was funded totally by the Laboratory Director's fund.

Rome Air Development Center
Air Force Systems Command
Griffiss Air Force Base, NY 13441-5700

This report has been reviewed by the RADC Public Affairs Division (PA) and is releasable to the National Technical Information Service (NTIS). At NTIS it will be releasable to the general public, including foreign nations.

RADC-TR-90-177 has been reviewed and is approved for publication.

APPROVED: Charles K. Makekau

CHARLES K. MAKEKAU, 1LT, USAF
Project Engineer

APPROVED: Harold Roth

HAROLD ROTH
Director of Solid State Sciences

FOR THE COMMANDER: James W. Hyde III

JAMES W. HYDE, III.
Directorate of Plans & Programs

If your address has changed or if you wish to be removed from the RADC mailing list, or if the addressee is no longer employed by your organization, please notify RADC (ESOP) Hanscom AFB MA 01731-5000. This will assist us in maintaining a current mailing list.

Do not return copies of this report unless contractual obligations or notices on a specific document require that it be returned.

REPORT DOCUMENTATION PAGE

Form Approved
OMB No. 0704-0188

1. AGENCY USE ONLY (Leave blank)	2. REPORT DATE	3. REPORT TYPE AND DATES COVERED
	August 1990	Final Aug 87 to Mar 90

4. TITLE AND SUBTITLE

FIBER OPTIC SYNTHETIC APERTURE INTERFEROMETER

5. FUNDING NUMBERS

C - F19628-87-C-0204
PE - 61101F
PR - LDFP
TA - 08
WU - C7

6. AUTHOR(S)

Michael Hercher

7. PERFORMING ORGANIZATION NAME(S) AND ADDRESS(ES)

Optra, Inc.
66 Cherry Hill Drive
Beverly MA 01915

8. PERFORMING ORGANIZATION REPORT NUMBER

N/A

9. SPONSORING / MONITORING AGENCY NAME(S) AND ADDRESS(ES)

Rome Air Development Center (ESOP
Hanscom AFB MA 01731-5000

10. SPONSORING / MONITORING AGENCY REPORT NUMBER

RADC-TR-90-177

11. SUPPLEMENTARY NOTES

RADC Project Engineer: Charles K. Makekau, 1Lt, USAF/ESOP/(617) 377-3488

12a. DISTRIBUTION / AVAILABILITY STATEMENT

Approved for public release; distribution unlimited.

12b. DISTRIBUTION CODE

13. ABSTRACT *(Maximum 200 words)*

This report describes a Fiber Optic Stellar Interferometer built by Optra, Inc. for the purposes of (1) measuring stellar diameters using a pair of small portable telescopes (rather than a large observatory telescope), and (2) measuring atmospheric turbulence. The key element of this concept is the use of singlemode optical fibers to link the separate small telescopes with the interferometer module. We have shown that the proposed turbulence measurements are entirely feasible using a distant light source (preferably a laser). The demonstration of the ability to obtain white light fringes through the fibers was not successful. We believe that this is due to a mismatch in the lengths of the fibers, and we have proposed a simple and flexible solution to this problem.

14. SUBJECT TERMS

Interferometer, Atmospheric Turbulence, Laser, Telescopes

15. NUMBER OF PAGES

56

16. PRICE CODE

17. SECURITY CLASSIFICATION OF REPORT	18. SECURITY CLASSIFICATION OF THIS PAGE	19. SECURITY CLASSIFICATION OF ABSTRACT	20. LIMITATION OF ABSTRACT
UNCLASSIFIED	UNCLASSIFIED	UNCLASSIFIED	UL

TABLE OF CONTENTS

LIST OF FIGURES

FIBER-OPTIC STELLAR INTERFEROMETER

FINAL REPORT & OPERATING MANUAL

1. OVERALL GOALS

The objective of this program was to build a fiber-optic version of a Michelson Stellar Interferometer and to demonstrate its ability to quantitatively measure both atmospheric turbulence (using a laser light source and a horizontal line of sight), and stellar diameters.

1.1 Turbulence Measurement

From an optical point of view, turbulence is a temporal variation in the refractive index of air along the path from an object to an optical system used to observe the object. Generally, spatial variations of refractive index accompany the temporal variations.

The effects of turbulence on image quality can be divided into two classes: image motion, and image degradation without motion. If we think of a point source, then in the case of turbulence-induced image motion the image of the point source actually moves in the image plane due to varying spatial refractive-index gradients. In the case of turbulence-induced image degradation, the image of the point source is enlarged (aberrated) due to wavefront distortions assoaciated with the turbulence. Both types of turbulence effect can and usually do occur at the same time.

From an operational point of view we can fully describe turbulence from an optical point of view in terms of a phase function $\phi(r,t)$, where r is a position coordinate in the aperture plane of the optical system and t is time. Referring to figure 1-1, we define this phase function as follows:

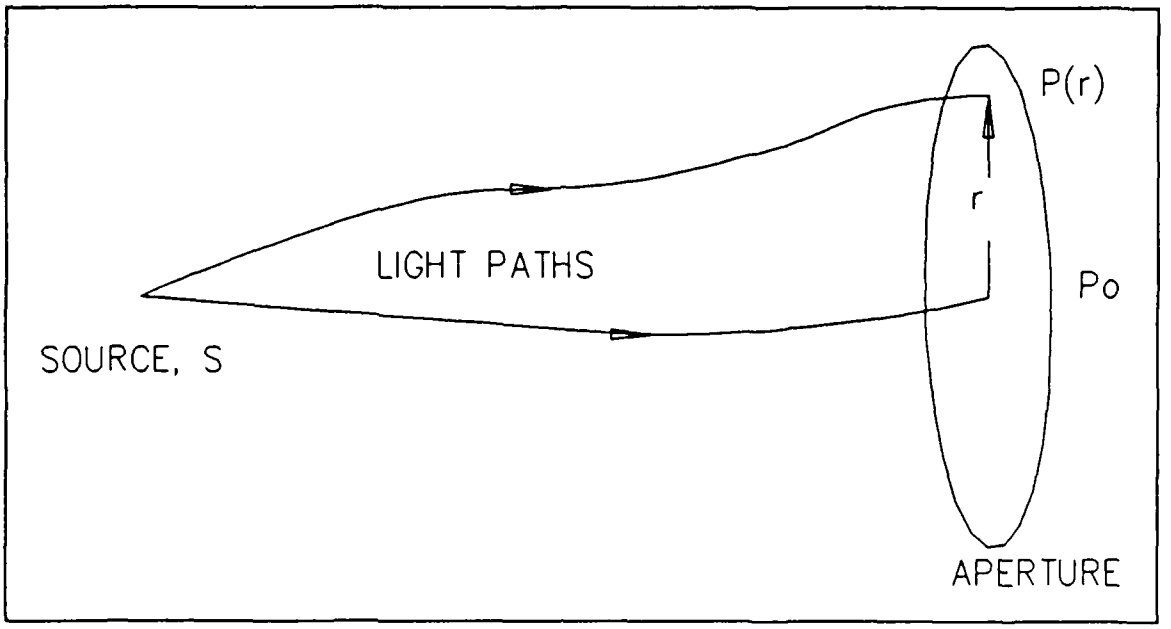

Figure 1-1 **Optical Paths for Defining Turbulence Effects**

Light travels from the source S to two points, P and P_0, in the aperture plane of the optical system. Turbulence may cause time-varying differences in these two optical paths. Severe turbulence may, as shown, distort the optical paths so that the source appears to move laterally when viewed from P and/or P_0.

(1.1)

$$\phi(r,t) = \frac{2\pi}{\lambda_0}\left(\int_S^P n(t)\,dl - \int_S^{P_0} n(t)\,dl\right),$$

where S is the point source, $P \equiv P(r)$ is a point in the aperture plane with vector coordinate r, $P_0 \equiv P(0)$, and λ_0 is the vacuum wavelength of the light. The integrals are line integrals, from S to P or P_0, of the refractive index of the air. (The actual path take by light going from S to P or P_0 will not generally be a straight line, but will be the path where the line integral of the refractive index has a local extremum.)

Within the aperture of an actual optical system, the points P and P_0 can be defined by actual physical masks (e.g. ¼-inch holes): an interference fringe pattern will then be formed in the image plane, and *phase* of the fringe pattern will have a 1:1 correspondence with the phase function $\phi(r,t)$ defined above. Temporal variations in the turbulence would produce corresponding variations in the positions of the interference fringes.

Figure 1-2 shows the basic layout of the Fiber-Optic Stellar Interferometer (FOSI) configured to monitor atmospheric turbulence. Two separate telescopes view a distant point source S (a laser is ideal because of its high brightness of narrow spectral bandwidth). Each telescope forms an image of S in its focal plane. Single-mode optical fibers collect the light from the image of the point source while a pair of servo-controlled galvo mirrors keep the images of S centered on the ends of the fibers. The optical arrangement for the galvos and servo detectors is shown in figure 1-3. The interferometer, whose function and design are described in detail in section 2, continuously measures $\phi(r,t)$, while the error signals from the galvos provide direct measures of any apparent angular displacements of the source due to turbulence.

The particular advantage of the use of singlemode optical fibers in this system is that it allows a large and variable separation between the points P and P_0 without the need for building a large interferometer to combine the light from P and P_0. The optical fibers provide a constant-path link between the widely separated points P and P_0, and a relatively small

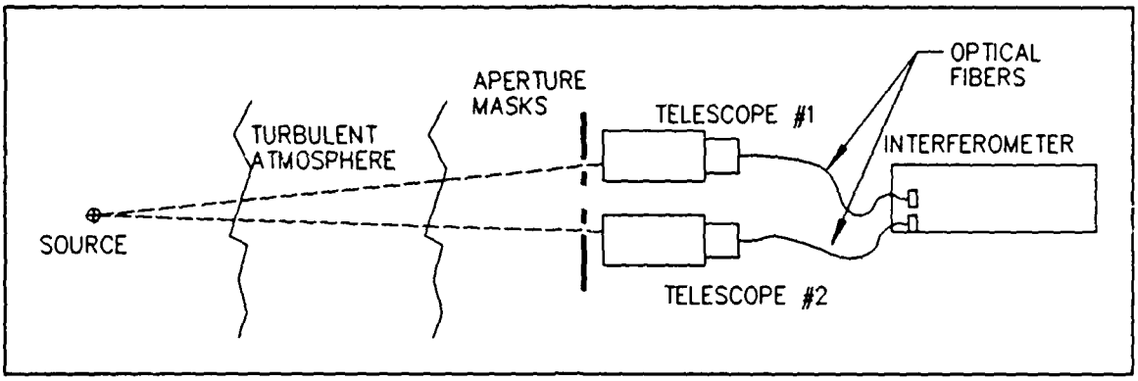

Figure 1-2 Optical Arrangement for Measuring Turbulence Effects

Light at P and P_0 is collected by separate telescopes (equipped with apertures if desired) and coherently transported to an interferometer via optical fibers. The two signals are combined at the interferometer and the phase of the resulting interferogram is monitored as a function of time in order to characterize the turbulence in terms of both the amplitude of the phase excursions, and their temporal frequency content.

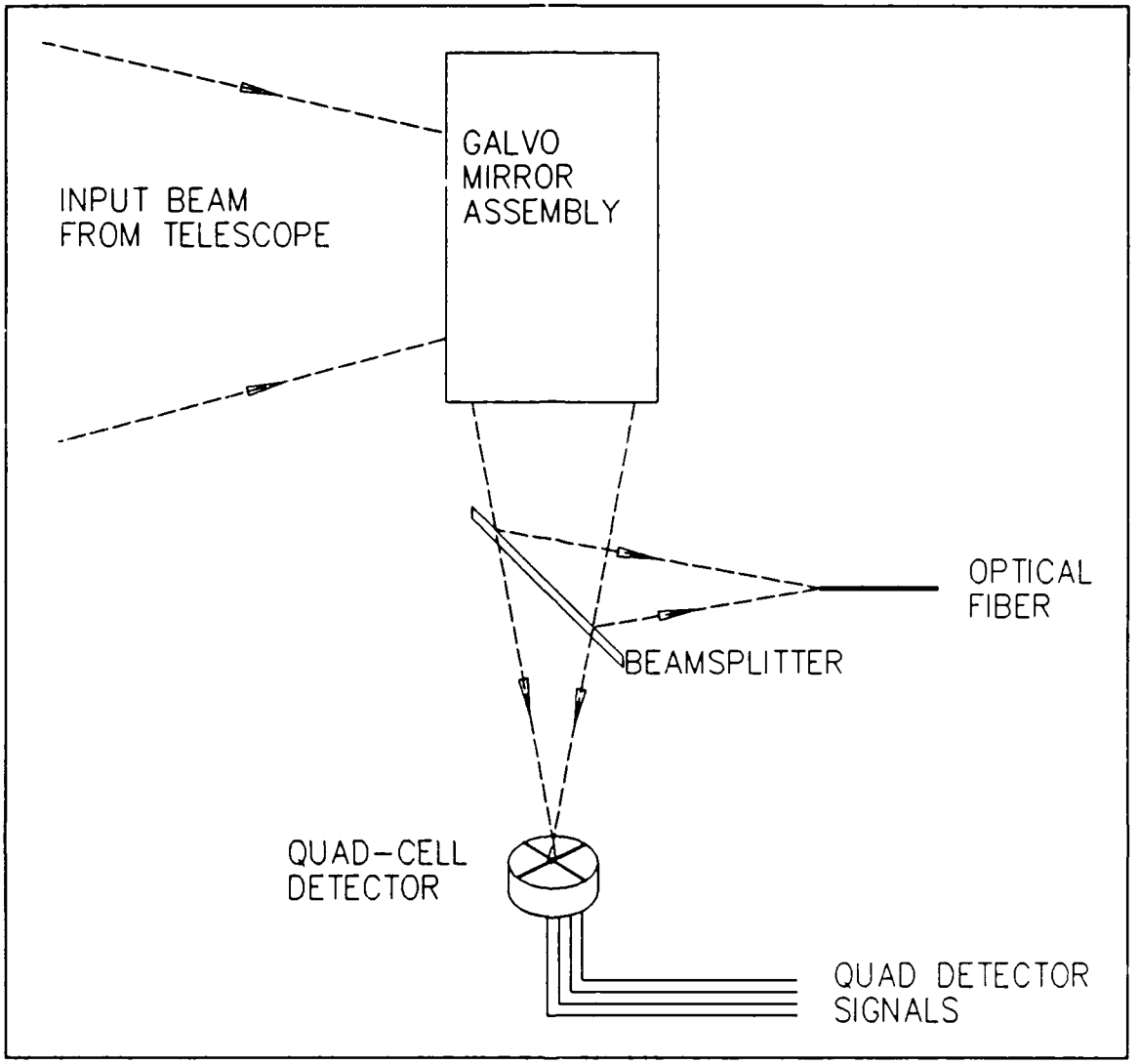

Figure 1-3 **Telescope Servo-Galvo Assembly**

The exit beam from the telescope passes through a dual galvo-mirror assembly which can position the exit beam in orthogonal angular directions. The exit beam passes through a beamsplitter which directs most of the signal to the singlemode optical fiber, and a portion of the signal to a quad-cell detector (silicon PIN-diode). Initially, the beam is positioned precisely onto the end of the fiber, and the quad cell is positioned to produce a null signal (equal signals from all 4 quadrants). Subsequent angular displacements of the beam generate error signals from the quad detector, which drive the galvo mirrors so as the null the error and reposition the image onto the end of the fiber.

interferometer which measures the turbulence-dependent path difference or phase.

1.2 Stellar Interferometry

As had been realized by Michelson, and expressed more precisely by van Cittert and Zernike, the angular intensity distribution of a small distant source and the complex degree of coherence measured at a large distance from the source constitute a Fourier transform pair. The complex degree of coherence, $\mu(r)$, is defined as a quantity whose magnitude is equal to the fringe visibility (in a Michelson interferometer setup) and whose phase is that of the fringe pattern (referenced to a phase of zero for $r \to 0$). If the phase can't be accurately measured, it can usually be estimated well enough to ascertain the intensity distribution with good precision (for a symetrical instensity distribution the phase is either 0 or π). Referring to figure 1-4 we can re-state this in more pedestrian terms: if the separation r between P and P_0 is just large enough that the visibility of the interference fringes goes to zero, then the angular subtense Θ of the star is approximately:

$$\Theta \approx 1.22\lambda/r. \tag{1.2}$$

For example, if a star has a uniform brightness and an angular diameter of 0.03 μrad, the fringe visibility would go to zero for a separation r between P_0 and P of about 22 meters (for visible light; $\lambda \approx 0.55\mu$).

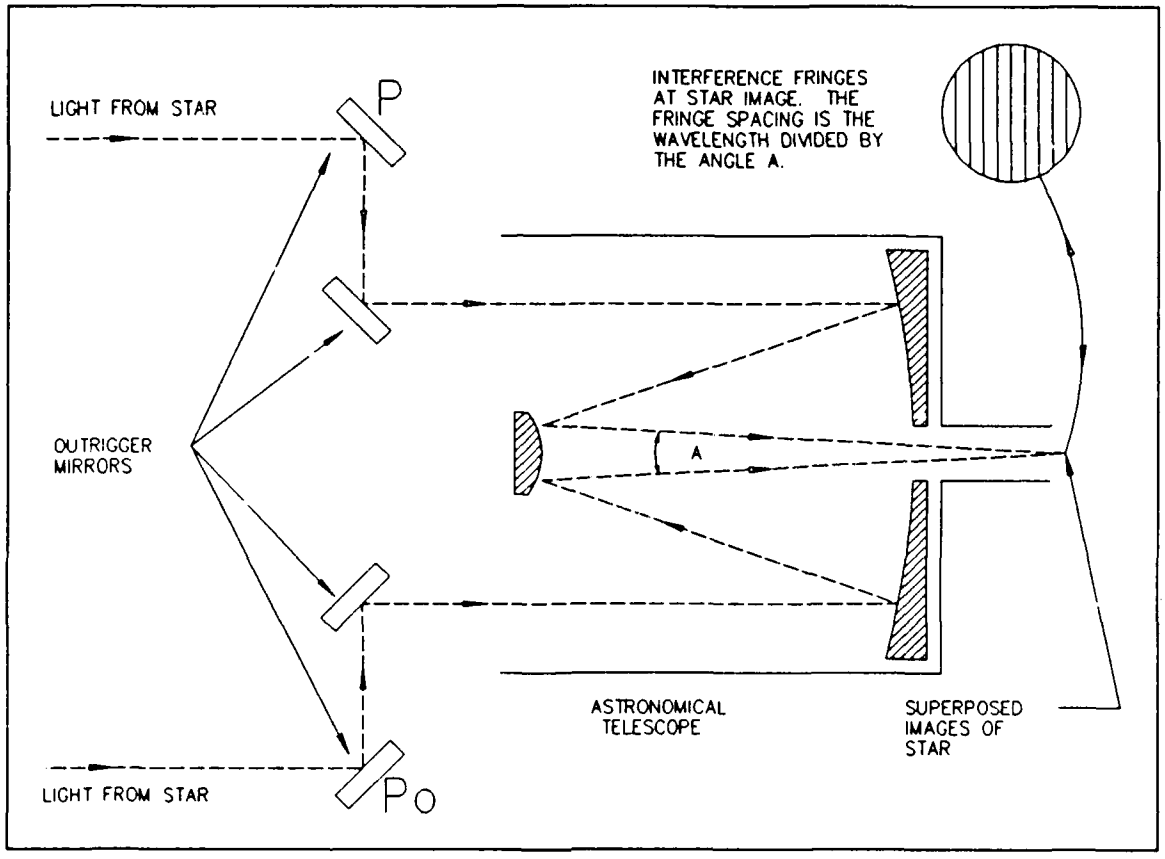

Figure 1-4 Layout of Conventional Michelson Stellar Interferometer

A spatial interference fringe pattern is formed as shown. A spectral bandpass filter may be used to increase the number of fringes (the number of fringes is approximately $\lambda/\Delta\lambda$, where λ is the wavelength and $\Delta\lambda$ is the spectral bandwidth). Turbulence will cause the fringes to move bak and forth. As the separation of the outrigger mirror is increased, the visibility of the fringes is reduced. If D is the separation of the mirrors when the visibility goes to zero, then the angular subtense of the star is on the order of λ/D.

2. CONCEPTUAL APPROACH

2.1 Conventional Michelson Stellar Interferometer

In a conventional stellar interferometer, such as that illustrated in figure 1-4, outrigger arms with mirrors are attached to a large astronomical telescope. Light is directed as shown to form a 2-beam interference fringe pattern in the focal plane of the telescope. The fringe visibility is recorded as a function of the separation between the outrigger mirrors and the Fourier transform of the resulting function then represents the radiance of the star as a function of angle. Turbulence and mechanical vibrations generally cause low-frequency movement of the interference fringes, and measurement of their phase is rarely if ever attempted. Spectral filtering may be used to relax the tolerence on keeping the optical paths (via the two mirrors) equal. The main function served by the large telescope is to guide on the star and to provide a rigid structure necessary for keeping the optical paths more or less constant.

2.2 Fiber-optic Stellar Interferometer

The Fiber-Optic Stellar Interferometer (FOSI), shown in figure 2-1, is intended to do the same job as a conventional stellar interferometer, but without the need for a large astronomical telescope. Instead, 2 small telescopes (e.g. 10" telescopes typically available--complete with equatorial mounts and tracking motor drive--for a few thousand dollars) separately track the star and the light beams collected by each are combined in a small, separate interferometer. The telescopes are linked to the interferometer by single-mode optical fibers, and the constancy of the optical path (as the telescopes separately track the star) is maintained by a servo-controlled mirror motion within the interferometer. The fringe pattern (whose visibility and phase carries the information) in the FOSI can be formed either spatially or temporally. We have chosen to use a temporal fringe pattern for a number of reasons:

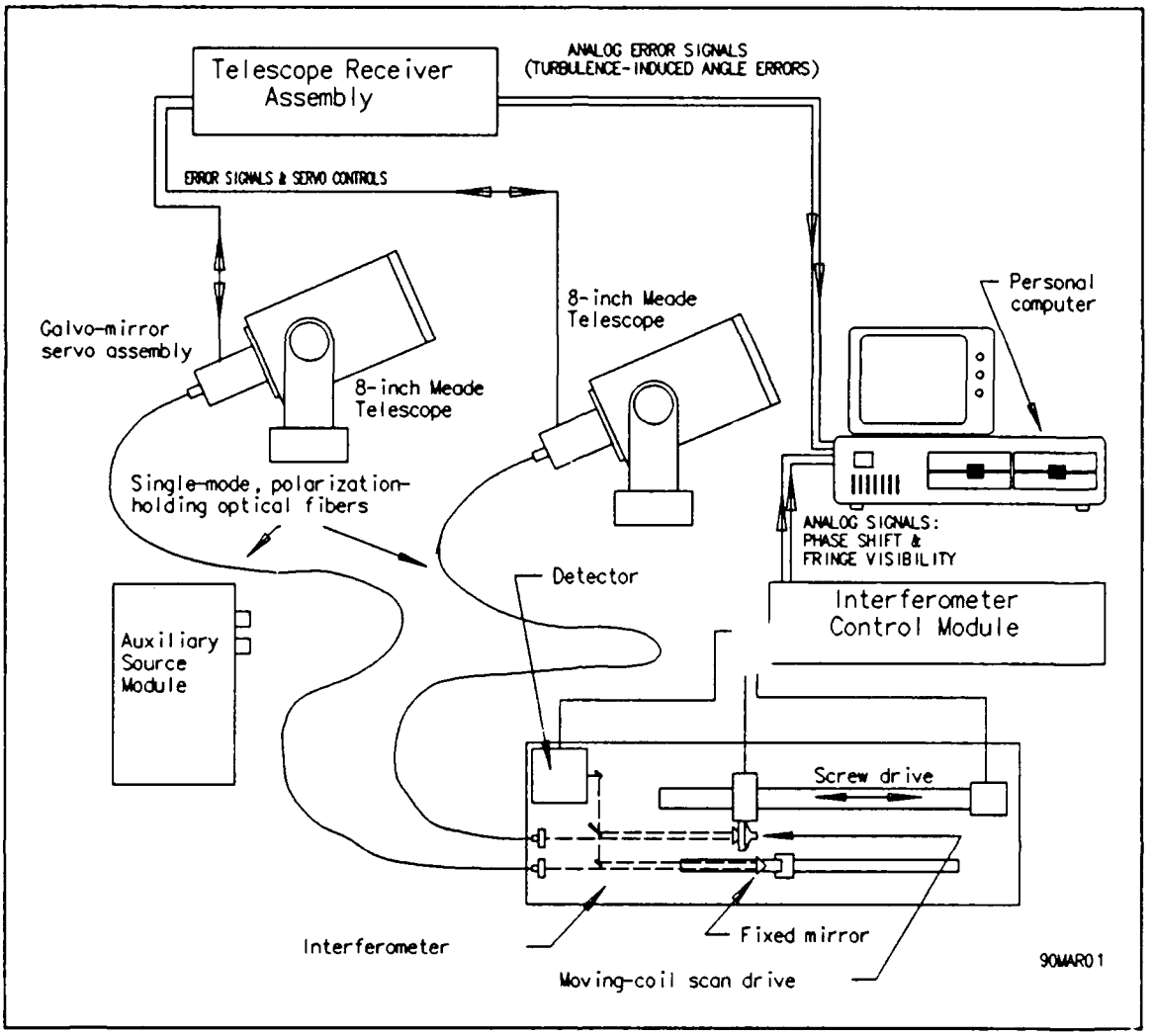

Figure 2-1 Complete Fiber-Optic Stellar Interferometer System

Separate small and independently steered telescopes replace the outrigger mirrors and large astronomical telescope shown in figure 1-4. Optical fibers provide a flexible but constant-optical-path link between the telescopes and the interferometer. Although the interferometer could produce a spatial interference fringe pattern, the light is far more efficiently used to produce a temporal interference fringe pattern. This is achieved by repetitively scanning one of the interferometer mirrors with a moving-coil transducer (i.e. loudspeaker).

- high radiometric efficiency--all the light goes into the signal;
- signal can be easily recorded with a single small silicon PIN diode detector; and
- convenient for scanning and servo control of optical path.

As shown in figure 2-1, the interferometer uses two corner-cube reflectors, so that their alignment is insensitive to small angular displacements. The upper corner-cube can be moved in two ways: (1) it can be moved over a range of about ±40cm by a variable-speed DC motor , and (2) it can be moved over a range of about ±15 microns by a moving-coil transducer (small loudspeaker) at frequencies up to a few hundred Hz. The moving coil transducer serves (a) to scan the mirror back and forth to generate the temporal fringe pattern, and (b) to make small low-frequency corrections to the position of the mirror--which are eventually picked up by the DC motor drive. (The DC component of the moving coil current is servo-controlled to keep the largest fringe in the center of the scan; the DC motor is servo-controlled to keep the DC moving coil current at zero).

A typical fringe pattern recorded with the FOSI would consist of a sine-squared wave under an approximately Gaussian envelope which enclosed on the order of 4 or 5 cycles of the sine-squared wave. The measurement of a stellar diameter would involve recording this fringe pattern for a set of different separations between the two telescopes. For each data run (which might take only 10 sec) the white-light fringe would have to be acquired, and the telescopes locked onto the star. By also recording the DC levels for each telescope separately, the fringe data may be properly interpreted in terms of fringe visibility.

2.3 Turbulence Measurements

For a turbulence measurement, the source may be a distant laser (pointed at the telescopes) or a bright narrow-band incoherent source (such as a mercury lamp). By using a laser, the precision with which the paths lengths must be made equal is greatly reduced--and S/N problems are virtually eliminated. The path along which the turbulence is measured extends from the telescopes to the source. Because of the cellular structure of the atmosphere, the measured turbulence is a function of the separation between two apertures for which the measurement is made. For stellar

viewing from terrestial sites in the visible, a general rule of thumb is that on a good night turbulence effects are negligible for separations less than about 25 cm. This means that diffraction-limited viewing may be possible for telescope apertures up to 25 cm (10-inches), but not much greater. In our experience this limiting aperture size increases monotonically with wavelength--at least out to 10 microns.

In setting up for a turbulence measurement, the two telescopes are positioned to define their separation d, and if necessary are equipped with small aperture stops. Both telescopes are aimed at the same distant source and aligned to maximize the signal levels at the output ends of the fibers. If the turbulence is enough to cause gross motion of the images (as opposed to degradation of the images without motion) the servo-controlled galvo mirrors should be activated. The error signals from the galvo mirrors will provide a record of the turbulence-induced image motion.

On a finer scale, the effect of turbulence is to introduce time-varying optical path differences along the two optical paths. This is manifest by an instability in the phase of the fringe pattern which is recorded when the interferometer mirror is cyclicly scanned--as illustrated in figure 2-2. For our purposes the turbulence is fully characterized by records of both the amplitude and frequency content of the fringe pattern excursions as a function of aperture separation, d. The interferometer has been equipped with a servo system which keeps the mirror scan centered on the peak of a specific fringe which is selected at the time the measurement is initialized. The error signal from this servo system contains all of the necessary data: it represents the optical path difference for the two apertures as a function of time. Turbulence-induced path differences may occur with amplitudes of up to 10 or 20 wavelengths and at frequencies of up to a few tens of Hz or less. By scanning the mirror at several hundred Hz, the scan-induced path differences can be easily filtered out. It may also be possible to identify (and filter out) lower frequency components which are due to meachanical resonances in the telescope mounts: any narrow peaks in the spectrum of the error signal will probably be associated with such mechanical vibrations.

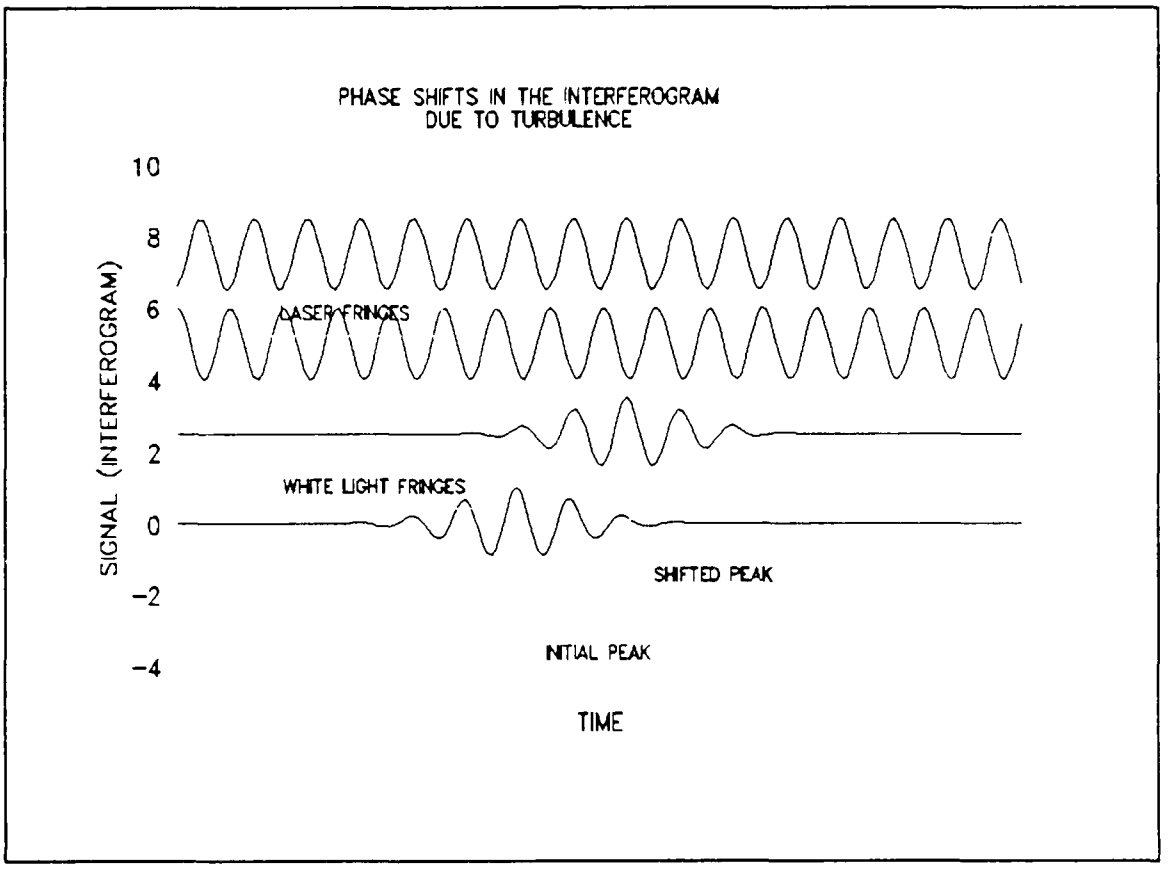

Figure 2-2 **Fringe Shifts due to Turbulence**

These figures represent the types of interferograms that might be recorded at two different times in the presence of turbulence. The white light fringe locations show that the phase change between the interferograms is about 3 cycles (corresponding to a path difference of 3 wavelengths). The laser fringes only give *modulo* 2π information in the recorded interferogram, but only a fringe has been locked only, the error signal provides a large dynamic range and allows large phase excursions to be followed.

3. THEORY OF OPERATION

3.1 Fiber-Optic Michelson Stellar Interferometer

The FOSI is in fact a combination of both the Michelson Stellar Interferometer and the conventional Michelson interferometer--with singlemode fiber-optics links between the telescopes and the interferomoeter. No new theory is involved for the interferometers, although the optical fibers warrant some further consideration.

A critical requirement for observing white-light fringes in an interferometer is that the optical path difference be zero--for all wavelengths. If the optical paths are entirely in air, then making the optical paths equal for one wavelength achieves equality at all wavelengths since the dispersion (variation of refractive index with wavelength) of air is so low. If, on the other hand, part of the path is in glass and part of the path is in air, the equalization of the optical paths at one particular wavelength does not in general assure that the paths will be equal for other wavelengths. The problem is the significant dispersion of glass. If the air paths are L_1 and L_2 and the glass thicknesses are T_1 and T_2, then the condition for path equality at a wavelength λ_1 is:

$$(3.1) \qquad n_a(\lambda_1)L_1 + n_g(\lambda_1)T_1 = n_a(\lambda_1)L_2 + n_g(\lambda_1)T_2.$$

To achieve this equality one of the air paths, say L_2, is made variable. The problem is that if T_1 and T_2 are not precisely equal the path difference will be a function of wavelength:

$$(3.2) \qquad \Delta OPD = (dn/d\lambda)\cdot\Delta L\cdot\Delta\lambda,$$

where $(dn/d\lambda)$ is the dispersion of the glass. It is a straightforward matter to calculate the white light fringe pattern for the case where there is a mismatch in the glass paths in the two arms of the interferometer. The parameters which enter into this calculation are (1) the glass thickness mismatch; (2) the dispersion of the glass; (3) the spectrum of the source and (4) the spectral sensitivity of the detector (including the spectral transmission of the optical system). Figure 3-1 shows computed white-light fringes

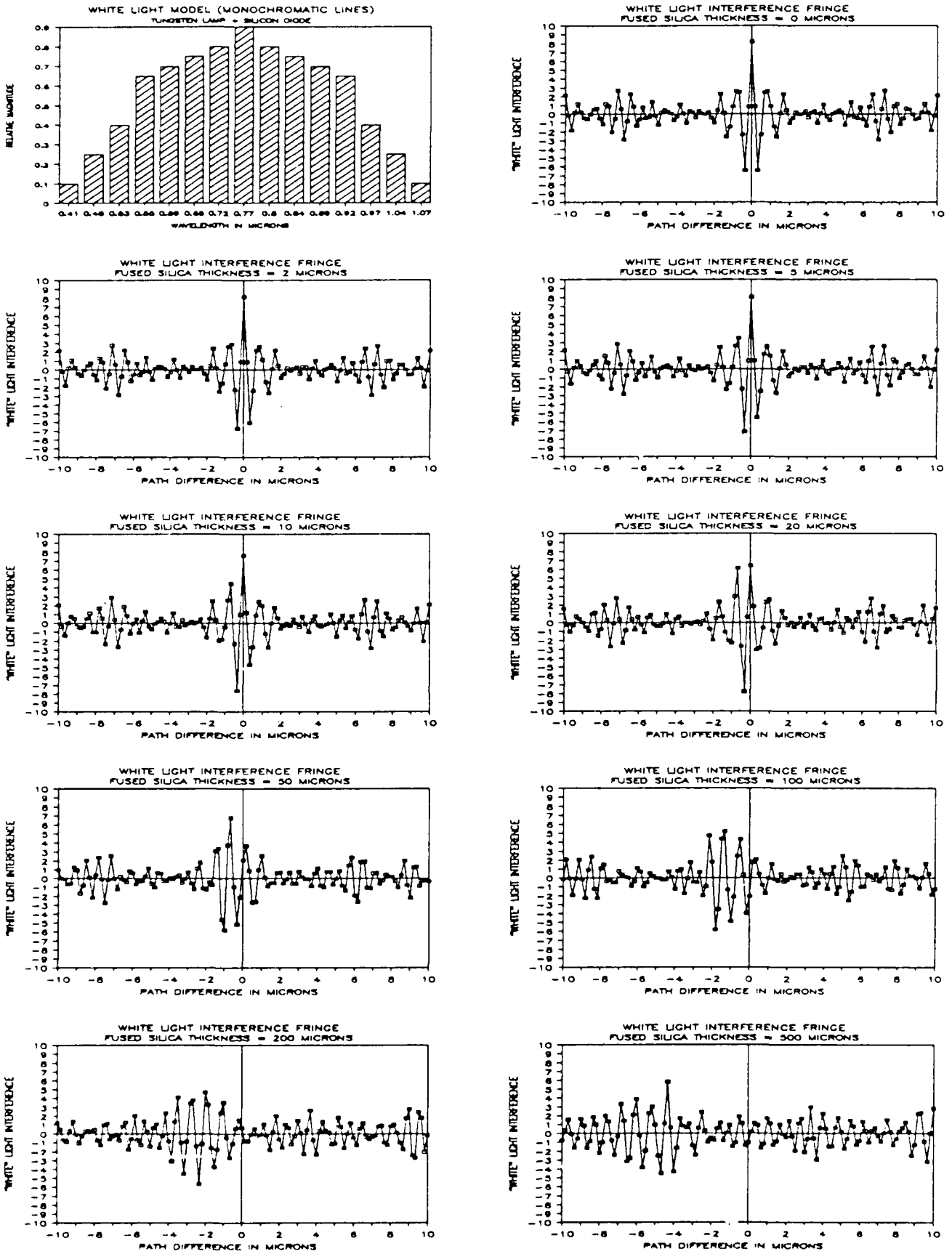

Figure 3-1 White Light Fringes with Dispersive Media

for a number of different thickness mismatches– assuming that the glass is fused silica and that the product of the source spectrum and the detector sensitivity are as shown in the first plot (at the upper left). From these data it is clear that when the thickness mismatch exceeds a value in the range of 50 to 200 microns, then the concept of a single well-defined white-light fringe is no longer viable.

This is a particularly critical problem in our case–where there is on the order of 60 meters of singlemode fiber in each arm of the interferometer. A 100 micron error in the length of one of the fibers is only 0.00016%, or 1 part in 600,000. Using time-of-flight techniques with short pulses from a laser diode it is in principle possible to match the fiber lengths with this type of precision. However, even small temperature differences between the two fibers might introduce enough perturbation to the optical paths to cause the loss of the white light fringe.

Interferometer Configuration and Alignment: as shown in figure 2-1, the FOSI looks quite similar to a conventional Michelson interferometer, except that it has two input beams and uses the beamsplitter to combine the beams to produce the interference. The two beams are fed in separately from the two telescopes via polarization-holding singlemode fiber. The polarization axes of the two fibers are aligned to be parallel both at the telescope ends (to insure that both beams are sampling the same state of polarization from the source) and at the interferometer ends (so that the beams will interfere with maximum contrast.

Both beams traverse paths within the interferometer which can be adjusted in length. Each arm uses an open corner-cube reflector with a lateral offset (see figure 2-1). In one arm the corner-cube can be moved along a 60 cm long track and locked into position with a screw; this corner-cube is provided with fine adjustments in X, Y and Z over a ± 3mm range. In the other arm of the interferometer the corner-cube is mounted onto a moving coil transducer (loudspeaker) with a maximum motion range (at low frequencies) of approximately ± 2.5 mm. The moving coil transducer, in turn, is mounted on a 70 cm long DC motor driven slide which can be driven at variable speeds up to 2.5 cm/sec. This configuration allows a

range of optical path differences of ± 1.3 meters, and provides the means for dithering and continuously tracking a given fringe peak over this full range.

The angular mirror adjustments of the input beams and the interferometer mirrors allow the two beams to be made parallel at the output of the interferometer, and the X and Y adjustments of the 'fixed' corner-cube allow the beams to be precisely superposed. It is a straightforward matter to align the interferometer and get high-contrast (> 90%) fringes from a laser source (which fully demonstrates the viability of the interferometer including fiber optics—without addressing the issue of equalizing the optical paths at all wavelengths of interest).

Path Equalization: we do not know at present the precise extent to which the optical fibers are (1) equal in length, or (2) identical in their dispersion characteristics. In our last attempt to equalize the lengths of the fibers, they were sent to York Ltd. (the manufacturers of the fiber, and probably the most capable company in state-of-the-art optical fiber technology) where after lengthy tests (in which temperature stabilization proved to be a critical factor) they were able to adjust the length of one of the fibers and certify that they were mismatched in length by 0.75 mm ± 0.25 mm. This should be marginally OK for white light, and should give good fringes for a spectrally narrower source—such as an LED.

In fact, we have never observed white light fringes. We have gotten workable white light signals through both fibers and have measured these light levels at the interferometer detector, but no fringes. Our strategy for finding the white light fringe was to equalize the paths as well as possible based on geometrical measurements, which we can certainly do to ± 2.5 cm, and to then slowly scan the moving mirror over the 5 cm range of uncertainty—having first made sure that high contrast fringes were obtained over the same scan range using a HeNe laser source (ensuring that the interferometer alignment was good over the full range). This is one of those situations where if the results had been positive, we could say with assurance that the fiber lengths were equal to within the necessary tolerance, the integrated dispersions of the fibers were equal, the stress-birefringence in the fibers had no significant effect, and the interferometer

alignment was good. In the absence of positive results, all we can say with certainty is that the interferometer alignment was good.

A Fix for Unequal Fiber Lengths: figure 3-2 illustrates a proposed fix which will allow the equalization of the fused silica thicknesses in the two arms of the interferometer. It assumes that these thicknesses start out by being unequal by no more than 1.5 mm, and provides a means for introducing a variable additional fused silica thickness difference which can be controlled over a range of ± 1.5 mm. If the problem is in fact due to a thickness mismatch (and not, for example, due to dispersion mismatches, temperature differences or stress effects which can't be corrected by a thickness correction), then this technique–combined with an appropriate white-light fringe search strategy–should do the job. Note that the ability to create a good white-light fringe is relevant only to the stellar diameter measurements: turbulance measurements are best made using a laser light source. In fact, even the stellar diameter measurements can be made without a good white-light fringe, providing a bandpass spectral filter can be used without excessive degradation of the signal level (in the stellar diameter measurement it is only necessary to record the fringe visibility as a function of telescope separation: being able to identify the zero-order fringe is not essential).

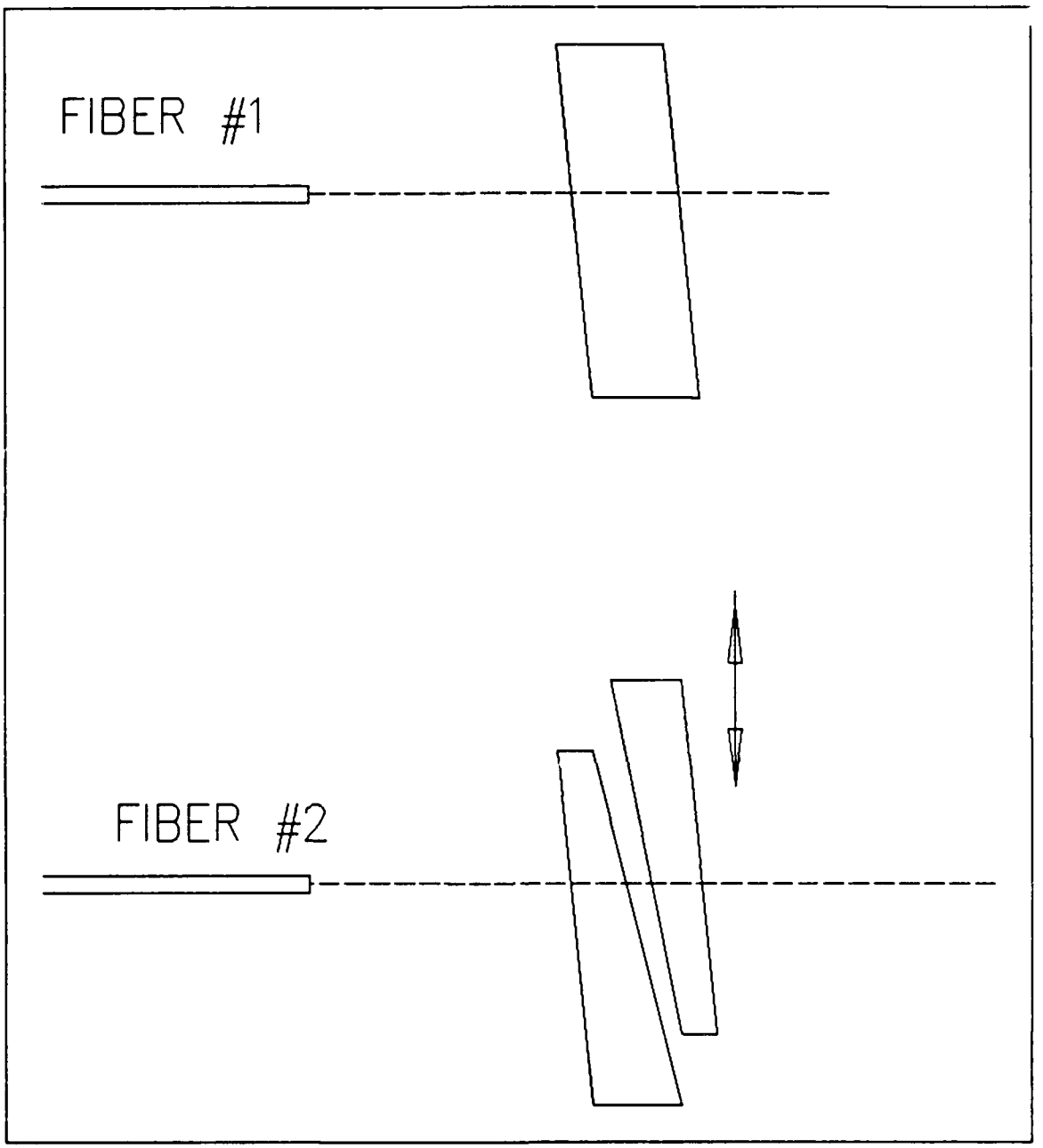

Figure 3-2 **Fused Silica Compensating Wedges**

As illustrated above, the wedges can be moved relative to one another to provide a very closely controlled fused-silica path difference between the two beams. This can be used to compensate for the difference in length between the two optical fibers (made of fused silica) in order to obtain white light fringes of high contrast.

4. DETAILED SYSTEM DESCRIPTION

4.1 Overall System Block Diagram

Figure 4.1-1 shows a block diagram of the complete system. Its key components are the following:

- 8-inch REFLECTING TELESCOPE with attached TELESCOPE RECEIVER ASSEMBLY, which includes dual servo-controlled galvo mirrors and a quadrant detector for sensing image motion (Qty 2).

- TELESCOPE TRACKING ELECTRONICS, which generate error signals for the galvos (to keep the star image centered on the optical fiber) and generate analog output voltages to provide a measure of both turbulance-induced image motion and systematic motion of the image (Qty 2).

- SINGLE-MODE POLARIZATION-HOLDING OPTICAL FIBER, approximately 60 meters in length, to coherently link the telescope assemblies with the interferometer. Each fiber has a core diameter on the order of 5 microns and the two fibers are matched in length to a fraction of a millimeter (Qty 2).

- INTERFEROMETER ASSEMBLY with connectors for the optical fibers, dynamically adjustable mirrors to track a fringe as the optical path difference changes, static adjustments to optimize alignment, and a sensitive detector for detecting fringe signals (Qty 1).

- LIGHT SOURCE MODULE containing both a HeNe laser and a quartz-tungsten-iodine incandescent lamp. This module has two connectors for the telescope ends of the optical fibers; it serves to get either monochromatic or white light into the fibers without the need for the telescopes and related assemblies. It is an ideal tool for setting up the interferometer and for verifying its alignment. The connectors are keyed so that the

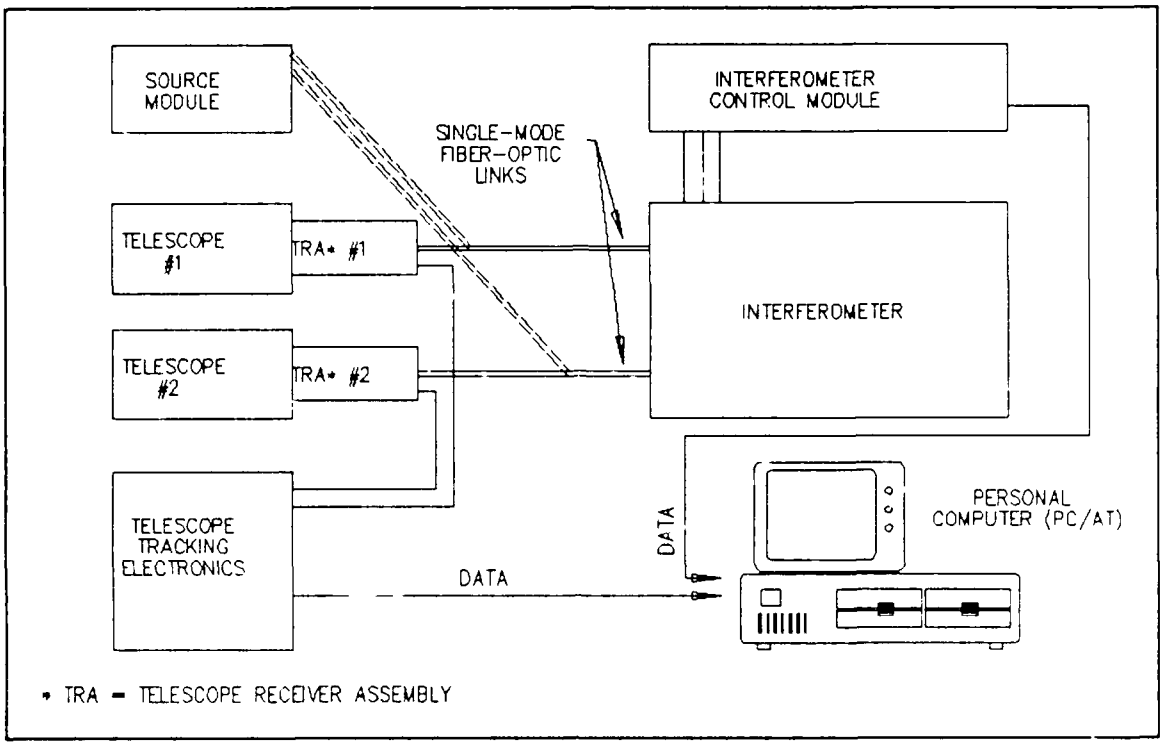

Figure 4.1-1 **Overall FOSI System Block Diagram**

polarization axes of the fibers are always correctlu oriented with respect to one another.

- INTERFEROMETER CONTROL MODULE. This module processes the data from the interferometer detector, and generates low-frequency error signals to the DC-motor drive and moving-coil transducer to keep the interferometer locked onto a specified fringe peak. It provides a relatively high-frequency dither to the moving mirror to allow the fringe peak location to be continuously monitored. It also generates analog output signals which are proportional to the position of the moving mirror (and hence to the instantaneous path difference) and to the contrast (or visibility) of the fringe pattern (Qty 1).

- PERSONAL COMPUTER (286 OR 386) (not supplied by OPTRA). The output signals are well suited for logging, display and preliminary interpretation by a PC. The computer should be equipped with a multichannel A/D board such as that manufactured by MetraByte. Software such as LabTech Notebook or Lotus 123 should be adequate for post-detection data-processing and display.

These separate modules are described in more detail below.

4.2 Telescope Receiver

The telescope receiver consists of a Meade telescope modified by the addition of a receiver assembly (OPTRA #103594), as illustrated in Figure 4.2-1.

4.2.1 Telescope

The telescope is an 8" Schmidt-Cassegraim telescope, Meade Model 2080. The telescope includes a field tripod and an equatorial wedge. Refer to Meade Instruction Manual for a detailed description of the telescope.

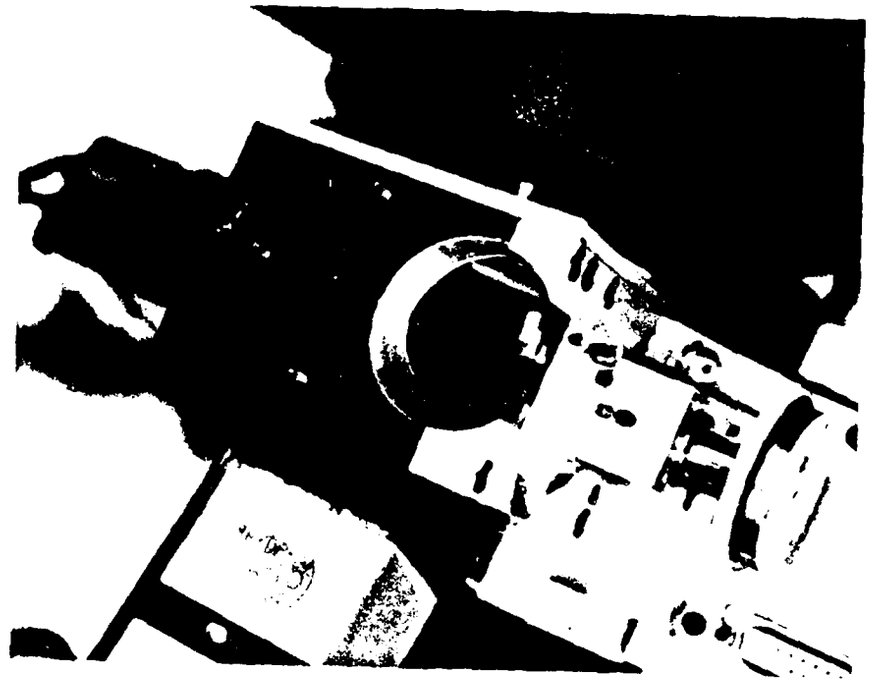

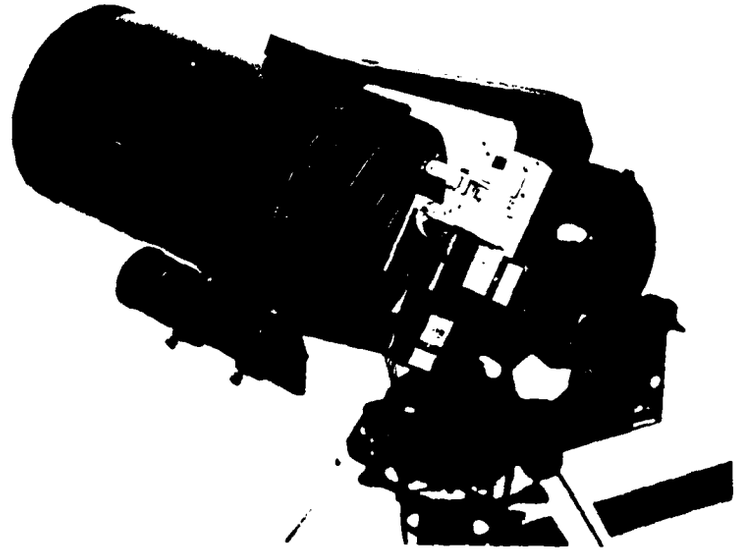

Figure 4.2-1 Receiver Assembly

4.3 Receiver Assembly

The receiver assembly consists of a General Scanning Inc. X-Y Scan Head Model 1013, a quad detector preamp assembly (OPTRA #104352) mounted on a frame which bolts into the rear of the Meade Telescope in place of the eyepiece. Also on the frame is an assembly which focuses the light from the telescope onto the tip of a fiber optic cable.

4.4 Galvo Servo Loop

The Galvo servo loop is designed to keep light entering the telescope focused on the fiber optic as the angle between the telescope and the optical source changes. Figure 4.3-1 is a Block Diagram of the servo loop.

Light from an optical source is deflected by the X-Y Scan Head onto a beamsplitter (OPTRA #401591). The central portion of the light bundle passes through the beamsplitter to the fiber optic focusing lens. The outer portion is reflected and focused onto a quad detector array mounted in the detector preamplifier. The detector preamplifier generates two (2) error signals proportional to the difference between the center of the focused spot of light and the center of the quad cell array. These error signals are integrated and fed to the galvo drive amplifier inputs. When the servo loop is enabled these error signals are nulled. As the angle between the telescope optical axis and the optical source changes the X and Y scan head galvo angles are changed keeping the light centered on the quad cell and on the fiber optic lens.

An enable/disable control is provided. When disabled the galvos are at their mid-position. Two (2) potentiometers are provided which allow the galvo position to be adjusted. A signal proportional to the sum of the signals on the quad cell is applied to a threshold comparator circuit. When insufficient light illuminates the quad cell, the loop is disabled. An indicator light is illuminated when the loop is enabled.

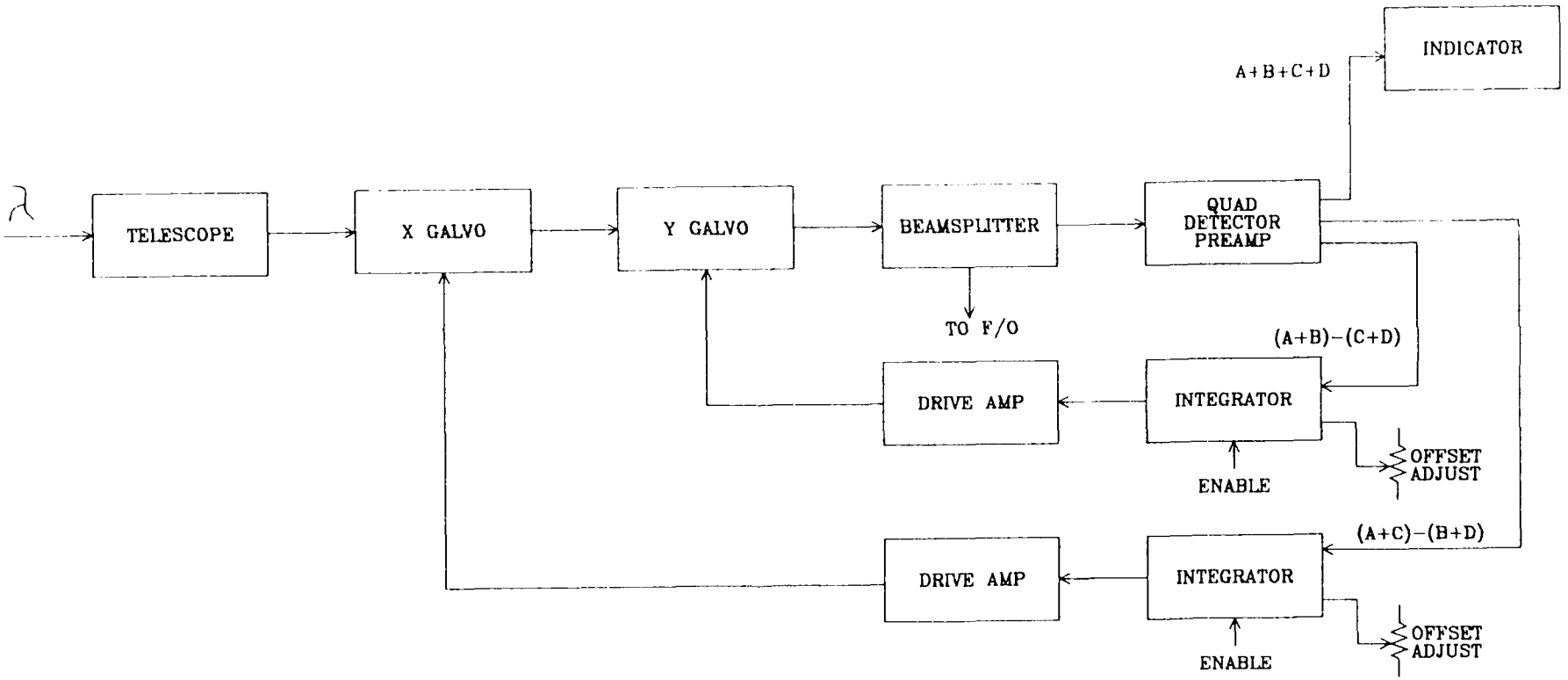

FIGURE 4.3−1
STELLAR INTERFEROMETER
RECEIVER GALVO SERVO LOOP BLOCK DIAGRAM

The servo electronics circuits were added to the General Scanning Inc. Scanner Control Amplifier chassis as illustrated in OPTRA drawing #501442.

4.4.1 Quad Detector - Preamplifier Assembly

The quad detector preamplifier assembly is a PC board assembly mounted in a shielded box. The detector array is a Hamamatsu S1557, a silicon photodiode 1 mm in diameter, divided into quadrants.

The circuitry includes four (4) transimpedance amplifiers and differencing amplifiers which generate X and Y error signals

$$X = (A + B) - (C + D)$$
$$Y = (A + D) - (B + C)$$

where A, B, C, D are the outputs of the four (4) transimpedance amplifiers.

The transimpedance amplifiers are Analog Devices AD549L electrometer amplifiers with 10^{10} OHM feedback resistors. Responsivity of the transimpedance amplifiers are 3×10^{9} volts/watt. The AD549L was chosen for its low bias current of $\approx$ 40 femptoamps, low offset voltage of 300 microvolts. Noise equivalent power is approximately 5×10^{-15} Watts RMS/$(HZ)^{1/2}$.

Two (2) voltage regulators provide stable ± 7 VOLTS DC to the AD 549L op amps. The differencing amplifier op amps are powered by ± 12 VDC from the galvo electronics chassis.

The detector preamp assembly is designed to detect a change of 2μM on the detector array of the source at a power level on the detector of 2×10^{-10} Watts.

OPTRA drawings 104343, 104253, 501484 and 501453 detail the design. Test results of SN001 assembly are:

- Dark noise @ 200 Hz: 16 microvolt RMS/(HZ)½

- Dark offset voltages 200 → 400 microvolt DC
- Bandwidths 106 HZ minimum

4.5 Optical Fibers

The single-mode polarization-holding fibers were made by York Ltd. and are equipped with single-mode connectors made by xxxx at both ends. At the connection point, both fiber ends are epoxied to GRIN lenses which produce a collimated beam. The connector has angular adjustments which allow the directions of the two collimated beams to be brought into coincidence. Lateral overlap of the two beams is assured by their relatively large diameter ($\approx$ 1 mm). Figure 4.5-1 illustrates the connector design. The connectors are equipped with keys which ensure consistent alignment of the polarizations axes of the fibers.

4.6 Interferometer Assembly

The interferometer layout is illustrated in figure 4.6-1 and is straightforward. It has proven easy to use and to align. The source module is especially valuable in this regard, since it allows the interferometer alignment to be optimized independent of the telescopes. The beamsplitter is a special component which was manufactured by Melles-Griot using their hybrid metal-dielectric coating which provides approximately 50-50 beamsplitting independent of the state of polarization. The interferometer alignment procedure is as follows:

1. Connect the optical fibers so that they link the source module and the interferometer module. Turn on the laser source in the source module and verify that there are laser beams emerging from the interferometer connectors. These beams should be collimated and about 1 mm in diameter.

2. If necessary, adjust the fiber-optic connector mounts on the interferometer so that the laser beams follow a path which is parallel to the interferometer mirror tracks (in both azimuth and altitude).

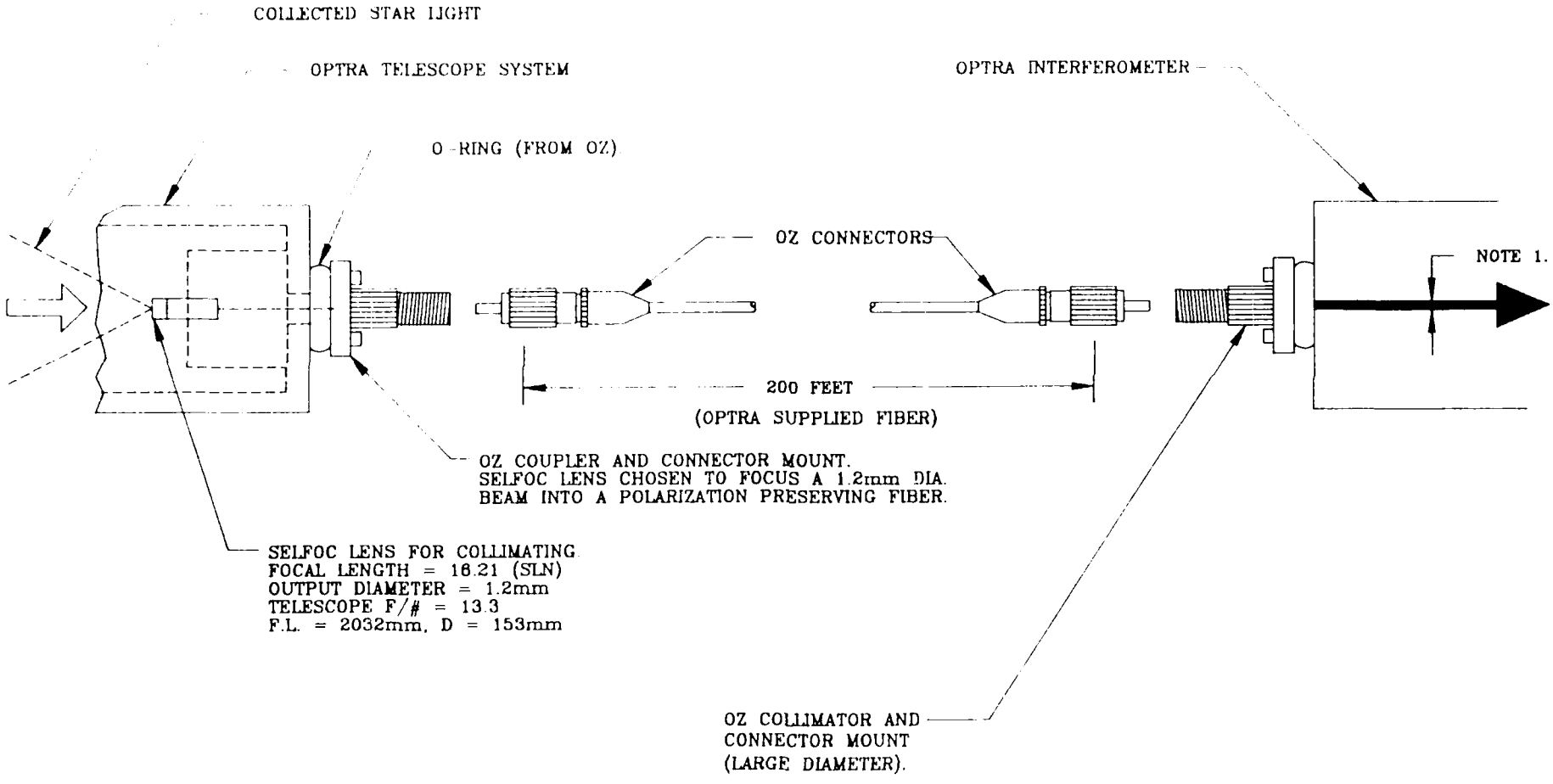

FIGURE 4.5-1 CONNECTOR DESIGN

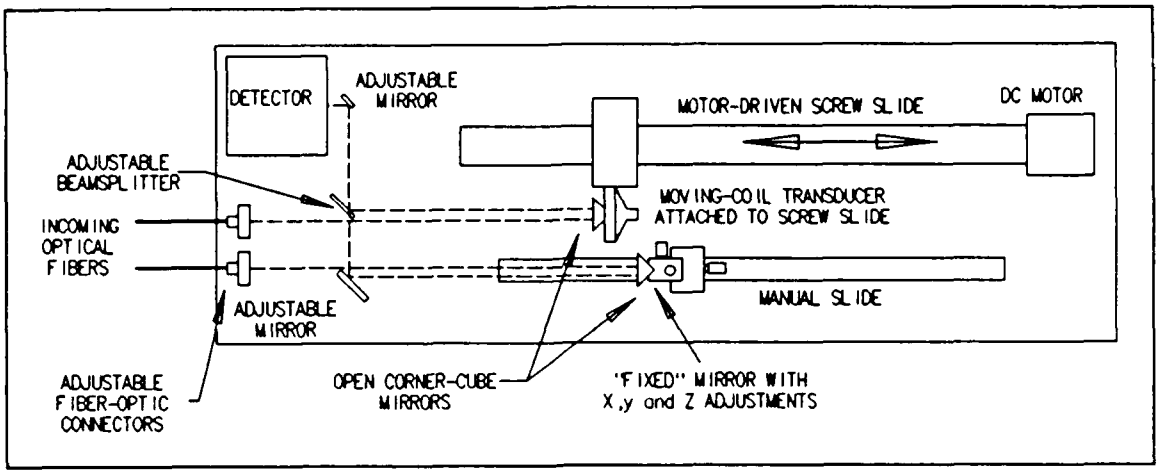

Figure 4.6-1 **FOSI: Interferometer Module**

When properly aligned, the beams leaving the interferometer should experience no lateral displacement when either corner-cube mirror is displaced longitudinally.

3. When properly aligned, the two exiting beams, from the two arms of the interferometer, should be parallel and superposed. The parallelism requirement is the more stringent of the two. Once the beams have been made parallel to the mirror tracks, the alignment procedure is:
    a. Adjust the last mirror before the beamsplitter, in the lower arm of the interferometer (figure 4.6-1), so that the reflected beam is superposed on the beam from the upper arm on the surface of the beamsplitter.
    b. Adjust the beamsplitter so that the two reflected beams (which are superposed in the plane of the beamsplitter) are superposed at some distance (5 or 10 feet) from the beamsplitter.
    c. Adjust the mirror between the beamsplitter and the detector so that the beams fall onto the detector.
    d. Make a fine adjustment to the beamsplitter to produce fringes in the output of the detector when a sinusoidal scan signal is applied to the moving-coil in the upper arm of the interferometer. Further adjust the lateral position of the beam (using the adjustments on the fixed cube-corner mirror) to maximize the fringe amplitude.

4.7 Interferometer Control Module

Figure 4.7-1 is a functional block diagram of the Interferometer Control Module electronics. The function of the control module is to detect and track a white light fringe from the interferometer and provide signals proportional to fringe contrast and changes in fringe position to be used to extract information about air turbulence. The module has three (3) operating modes: search, scan, and track.

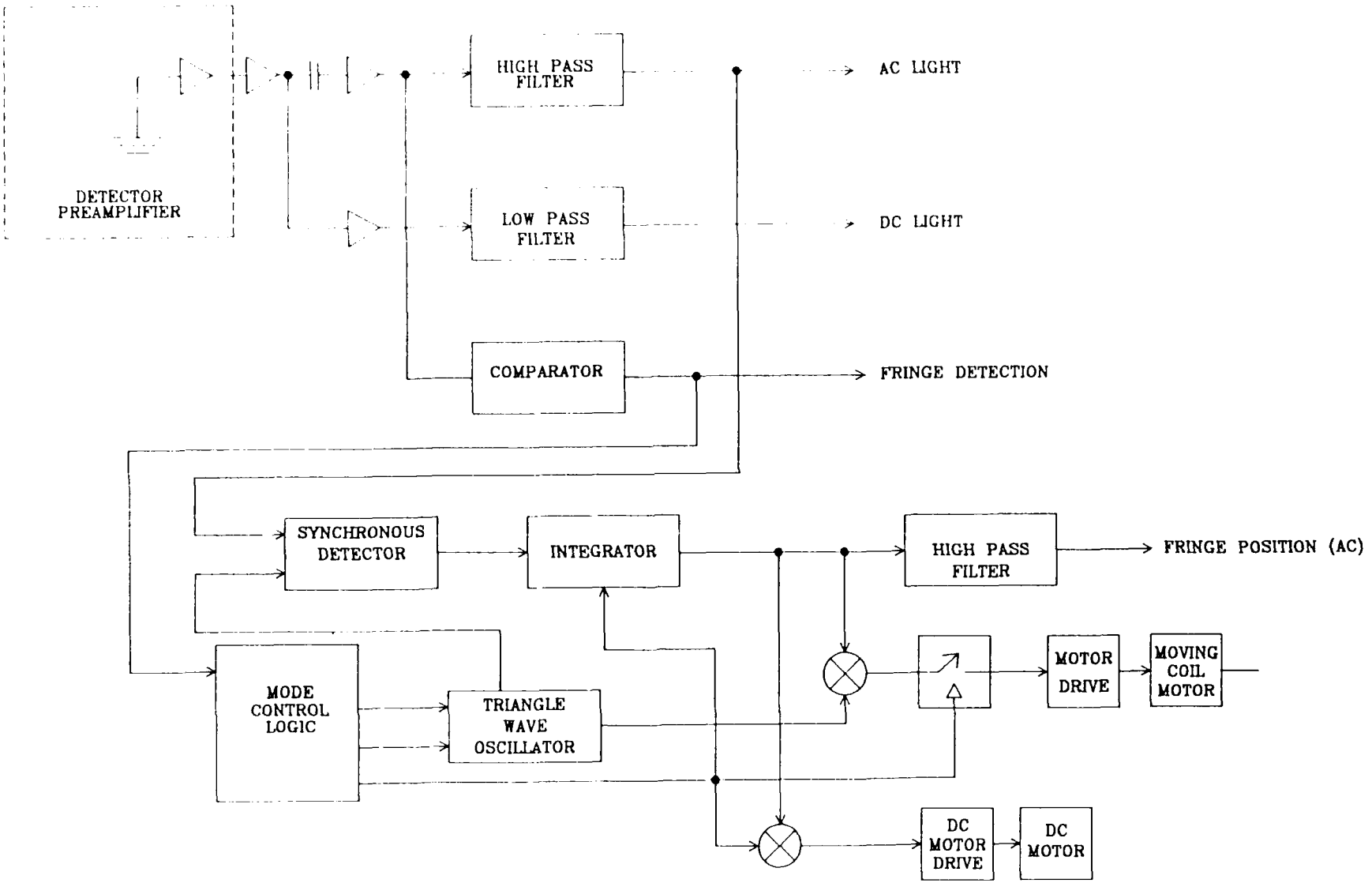

FIGURE 4-7-1
BLOCK DIAGRAM -- INTERFEROMETER CONTROL MODULE

In the search mode the interferometer DC motor is slowly scanned and the moving coil motor drive is disabled. A comparator circuit monitors the AC component of the detector output. As the moving arm of the interferometer driven by the DC motor passes through the zero path difference, a white light fringe is generated exceeding a comparator threshold. When the comparator threshold is exceeded, the mode control logic switches to scan mode. In the scan mode, the DC motor drive is disabled and the moving coil motor is enabled. The moving coil motor is driven by an amplifier whose output sums a triangle wave with an error signal derived from a synchronously detected signal from the detector.

This error signal drives the moving coil motor motion to be centered on the white light fringe. After five (5) seconds, the mode is switched to track. The amplitude of the moving coil motion is reduced by ≈ 10. At this point the moving arm of the interferometer is at zero path difference and the moving coil motor is dithering with the white light fringe centered on the motion. The loop error voltage which drives the moving coil motor is also applied to the input of the DC motor drive amplifier. This keeps the zero path difference of the interferometer within the useful range of the moving coil motor.

The loop remains enabled as long as the AC fringe signal exceeds the fringe detection comparator threshold. OPTRA drawing #581493 is the schematic diagram of the control module.

4.7.1 Hardware Status

The Interferometer Control Module has been assembled and bench tested. The component board has been installed in a 19" chassis. Chassis wiring is complete. The control module has not been integrated with the interferometer.

4.8 Laser & White Light Test Module

Early in the program it was realized that it would be very useful to have a source module, complete with fiber-optic connectors, which could be used to inject either laser light or white light into the singlemode optical fibers. Such a module was designed and built and is being delivered with the rest of the system as an alignment and diagnostic accessory. It contains a small HeNe laser, a miniature incandescent white light source & associated optics, and a series of mirrors and beamsplitters. Switches allow either source, or both, to be selected. The fiberoptic output couplers are prealigned for the two supplied fibers, but may be further aligned if desired.

5. OPERATING PROCEDURES

5.1 Turbulence Measurement

When a point source is viewed through a time-varying intervening medium, the effect of the medium may be thought of as a displacement of the apparent location of the source as viewed from the point of observation. Severe turbulence—producing significant refractive index gradients—may cause a lateral shift in the apparent position of the source. Weaker turbulence changes the optical path from the source to the observer, and may be thought of in terms of a longitudinal displacement of the apparent position of the source. The displacement may range from zero to a few tens of wavelengths, and must be sensed interferometrically. As described earlier, this is achieved by collecting light at a pair of laterally displaced points and monitoring the variations in the phase of the interferogram produced when the two beams are combined. Under the best seeing conditions for astronomical observations, turbulence effects are negligible until the separation between the two apertures is on the order of 30cm. For apertures larger than this figure, terrestrial diffraction-limited resolution is made impossible by turbulence effects.

A typical set of turbulence data would be comprised of short records (1 to 3 minutes in duration) of the phase difference between the two beams, recorded as a function of time with a 10 Hz resolution. These records would be obtained for different aperture separations and, presumably, under varied atmospheric conditions.

The experimental procedure is straightforward: using the laser source module, the interferometer is checked for alignment and maximum signal level. The telescopes are then position with the desired separation, and aimed at the distant (laser) source. The telescopes are aligned to maximize the signal out of the fiber-optic connectors. The fibers are then connected to the telescopes and the alignments touched up to maximize the signal levels at the output ends of the fibers. The voice coil is then activated by a (say) 100 Hz signal and the servo system is activated to lock onto a specific fringe. Data is now recorded simply by logging the servo error signal as a function of time. This error signal represents the mirror

displacement needed to restore the initial optical path difference, and is thus proportional to the turbulence-induced optical path difference.

5.2 Stellar Interferometry

In stellar interferometry it is necessary only to record the *interferogram visibility* as a function of the telescope separation; i.e. it is neither necessary nor useful to monitor or compensate for atmospheric turbulence. A measurement of a stellar diameter would consist of (a) recording the fringe visibility as a function of the telescope separation, and then (b) taking the tranform of this record in order to obtain the angular radiance profile of the star. As mentioned earlier, under the reasonable assumption that the star has a symetric radiance profile, the interferogram will always be real, and can be fully characterized by its visibility (contrast ratio). To this end, the interferometer module is equipped with an absolute value circuit which provides a low-frequency signal proportional to the AC amplitude of the interferogram. This, combined with the DC signal levels from each arm of the interferometer, provides full knowledge of the fringe visibility, V:

$$(5.1) \qquad V \equiv [I_{max}-I_{min}]/[I_{max}+I_{min}] = A/[2(I_1+I_2)],$$

where A is the AC signal amplitude and I_1 and I_2 are the separate DC light levels from the two arms of the interferometer.

Once the telescopes are both tracking (locked-on) the star and the white light fringe has been found, the visibility data can be recorded in a few seconds.

In order to find the white light (zero-order) fringe, the dispersive fiber lengths have to be equal and the optical paths through air have to be equal. This requires that the telescopes be set up so that they are equidistant from the star to within a few tens of centimeters. Given this situation, the moving mirror can then be driven by a simple search algorithm to find the white light fringe.

Since we were unable to obtain such a white light fringe—presumably due to an inbalance in the lengths of the fibers—further words of wisdom from us on this point must be viewed as somewhat suspect.

We are confident that once the interferometer is aligned and capable of observing white light fringes, it should be possible to move the mirror at up to 1.5 mm/sec without risking missing the white light fringe (this corresponds to a fringe frequency of about 5 kHz). Thus, assuming a maximum initial optical path error of ± 0.5 m, it should only take a maximum of about 10 minutes to scan the full range needed to acquire the white light fringe. The alignment would then the optimized (simply by maximizing the fringe contrast) and the AC and separate DC levels recorded with enough of a time constant to smooth out any temporal fluctuations. The process would then be repeated for the next value of the telescope separation.

6. EXPERIMENTAL DATA

6.1 Stellar Radiometric Signals

One Telescope Receiver Assembly was fitted with a prototype detector-preamplifier assembly. A silicon detector was coupled to a transimpedance amplifier with a gain of 1×10^9 volts/amp.

Various stellar objects were viewed and the preamplifier output recorded. The purpose of this experiment was to verify the radiometric calculations upon which the system design was based. Table 6.1 lists the results.

TABLE 6.1

Stellar Object	Volts	(1) Watts	(2) Watt/cm^2	(3) Expected Watt/cm^2
Vega	44 mV	1.5 E-10	5.4 E-13	4 E-13
Jupiter	512 mV	1.7 E-9	6.1 E-12	3 E-12
Mars	532 mV	1.8 E-9	6.5 E-12	3 E-12
Capella	47 mV	1.6 E-10	5.7 E-13	4 E-13

1. Detector/preamp responsivity = 3×10^8 volt/watt assumed
2. Telescope aperture = 8" diameter, 3" diameter obscuration, collection area = 278 cm^2
3. Expected irradiance estimated from Figures 6-7, 6-6 of RCA Electro-Optics Handbook. Does not include atmospheric losses or losses in telescope optics. Assumes 200 nm spectral bandwidth.

6.2 Interferometer Validation

Validation of the interferometer using the Optical Source Module was attempted unsuccessfully.

The Optical Source Module was connected to the interferometer through the two (2) single mode fiber optic cables. The cable lengths had been previously matched to 750 μ meters. Long and short axes were reviewed to insure the long axes were parallel. The path lengths in the Optical Source Module were measured and the movable leg of the interferometer was adjusted to nominal zero path difference. Alignment of the interferometer was verified by using the HeNe source in the Optical Source Module and dithering the optical path difference with the moving coil motor. A prototype detector-preamplifier was used to measure the light output. DC white light levels through each leg as well as the level of the overlapping light beams were measured as:

A = 4 E-10 watts
B = 4 E-10 watts
A + B = 6.7 E-10 watts

With the moving coil motor being dithered a small amount of a few microns, the moving arm of the interferometer was slowly moved by hand using a knob installed on the lead screw. Preamplifier output was monitored with both an oscilloscope and a spectrum analyzer.

An exhaustive search for the white light fringe over ± 5 cm from the nominal path difference was conducted with no sign of the white light fringe.

6.3 Turbulence Measurements

Turbulence measurements were made using the Light Source Module. A heated soldering iron was positioned below one of the beams in the source module: this heated the air above it it, causing a change in its refractive

index. This change could easily be observed as a phase shift the the fringe pattern recorded by the interferometer (see figure 2-2). By varing the distance between the soldering iron and the beam, the magnitude of the phase shift could be varied over a range of from 0 to 6 or 8 cycles. This phase shift would be quite steady in time. By blowing air into the source modules (or just waving a piece of paper over it) turbulence could easily be introduced. This would cause readily observable random motions of the fringe pattern with a magnitude on the order of 3 to 4 fringes and a mean fringe rate on the order of 1 or 2 Hz.

7. PROBLEMS & FIXES

7.1 No White Light Fringe: Use Fused Silica Wedges

As described in section 3 (page 10) we feel that a fused silica adjustable wedge arrangement would be well-suited for compensating for unequal optical fiber lengths (as well as for any mismatch in the thicknesses of the two halves of the beam splitter. The ideal place to locate these wedges (and the fixed plate for the unadjusted beam) would be on the interferometer base just following the fiber-optic connectors.

7.2 Galvo Servo Control

The assembly and alignment of the Telescope Receiver Assembly was unable to be completed successfully mainly because of difficulty installing and aligning the beamsplitter.

In order to transmit through the fibers a maximum of the light received by the telescope a beamsplitter was designed and fabricated that would transmit through a central hole (see Figure 7-2, OPTRA #401591). This design takes light from the outer zone of the entrance aperture (6" to 8" diameter) for the galvo tracker while using the central 6" aperture for the stellar signal at the interferometer. The original design mounted the beamsplitter on an adjustable mirror mount (OPTRA drawing #102841) which provided X and Y tilt adjustments for centering the reflected portion of the starlight on the quad detector. After many attempts to install a beamsplitter we decided to modify the design to add X and Y lateral adjustments for centering the beamsplitter hole on the star image from the telescope. This also proved unsuccessful leading to the conclusion that the beamsplitter could not be properly aligned without major redesign of the Receiver Assembly.

A solution to the above problem is to replace the beamsplitter with one that transmits and reflects. Although this design is not as efficient as the original design, the installation and alignment will be straight forward.

The existing mirror mounts will provide adequate X and Y tilt adjustment to position the reflected part of the light onto the quad detector.

8.0 LIST OF DELIVERED HARDWARE

The following is a list of hardware delivered under this contract.

1. Two (2) Telescope Assemblies - Meade type 2080 includes accessories, equatorial wedge and tripods.

2. Two (2) Receiver Assemblies; includes:

   - Two (2) General Scanning Inc. XY 1013 scan head assemblies
   - Two (2) General Scanning Inc. DX scanner control amplifiers - modified by addition of servo electronics
   - Two (2) cable sets
   - Two (2) quad detector preamplifiers
   - Two (2) cover assemblies

3. Two (2) single mode fiber optic cable assemblies - 200 meters long

4. One (1) Interferometer Assembly

5. One (1) Detector Preamplifier Assembly

6. One (1) Source Control Module

7. One (1) Motor Drive Control - manufactured by Minarik

8. One (1) Interferometer Control Module

8.1 Drawing List

The following is a list of drawings.

Drawing	Title
104423	Receiver Cover Assembly
104383	Quad Detector Assembly
103594	Receiver Assembly
103604	Focal Plane Assembly Layout
212654	Front Panel
501484	Circuit Board Assembly

Drawing	Title
212664	Rear Panel
212704	Cover Flange
212682	Mirror Mount Holder
212712	Telescope Cover
212732	Cover Strap
104342	Detector Preamp Assembly
104253	Detector Preamp Assembly
104412	Telescope Strap Assembly
211052	Beam Positioner Rework
211302	Nut - Rework
211352	Lens Cell
501493	Schematic - Interferometer Electronics Unit
211372	L.H. Gusset
211382	R.H. Gusset
211402	Shoulder
211432	Fiber Base
211452	Mirror Arm
211472	Shielded Box
211532	Handle Rework
212642	Shielded Box
211291	Knob - Rework
211341	Screw - Rework
211361	Mirror Mount Holder
211411	Eyepiece Clamp
211441	Mirror Lever

212591	Eyepiece Adapter
212671	Mirror Mount Adjust
401591	Beamsplitter
211281	End Plate
212761	Top Plate
211043	Detector Mount
211063	Filter Slide
211073	Filter Mount
211423	Adapter
212693	Receiver Cover
501453	XY Servo Board Assembly
501523	Detector Preamp Schematic
501473	XY Servo Board Schematic
501442	XY Galvo Electronic

Modifications

501433	Fabrication - Detector Preamp
501423	Schematic - Detector Preamp
102841	Adjustable Mirror Mount
209621	Mirror Mount
104352	Detector Preamp Assembly
212664	Rear Panel
212654	Front Panel

MISSION
of
Rome Air Development Center

RADC plans and executes research, development, test and selected acquisition programs in support of Command, Control, Communications and Intelligence (C^3I) activities. Technical and engineering support within areas of competence is provided to ESD Program Offices (POs) and other ESD elements to perform effective acquisition of C^3I systems. The areas of technical competence include communications, command and control, battle management information processing, surveillance sensors, intelligence data collection and handling, solid state sciences, electromagnetics, and propagation, and electronic reliability/maintainability and compatibility.